Chapter 15

Neutron Irradiation Effects in 5*xxx* and 6*xxx* Series Aluminum Alloys: A Literature Review

Murthy Kolluri

Additional information is available at the end of the chapter

http://dx.doi.org/10.5772/63294

Abstract

A literature review on highly irradiated 5*xxx* and 6*xxx* series Al alloys is conducted to understand the expected changes in mechanical properties of high flux reactor (HFR) vessel material in relation with microstructural aspects beyond the current surveillance data to support the HFR Surveillance Program (SURP). It was found that the irradiation swelling in 5*xxx* series alloys is not a crucial degradation mechanism. Dislocation damage is expected to reach a saturation limit in both 5*xxx* and 6*xxx* series alloys at relatively low fast-fluence values ($<2 \times 10^{26}$ n/m^2). The damage caused by precipitation of transmutation Si is found to be the dominant mechanism affecting the fracture toughness properties of irradiated 5*xxx* and 6*xxx* series Al alloys at high thermal fluence values. Tensile and fracture toughness data collected from the literature up to very high thermal fluences are analyzed in comparison with the available HFR surveillance data to predict the behavior of the HFR vessel material beyond current surveillance data. The observed changes in mechanical properties are classified into four different regimes. The contribution of various irradiation damage mechanisms, namely the displacement damage and transmutation damage, to the evolution of microstructure and mechanical properties is discussed in all four regimes for 5*xxx* and 6*xxx* series alloys.

Keywords: irradiation defects in aluminum alloys, displacement damage, transmutation damage, Mg_2Si precipitates, fracture toughness, radiation hardening, embrittlement

1. Introduction

Aluminum alloys have a higher tolerance to radiation effects than most other metals when irradiated at ambient temperatures due to its low melting point (T_m). This is because, at room

temperature, the homologous temperature of Al alloys is around $0.32T_m$, when compared to, for instance, ~$0.175T_m$ for austenitic steel, ~$0.17T_m$ for ferritic steel, and ~$0.14T_m$ for α-Zr. In metals, it is known that noticeable thermal diffusion of vacancies occurs at homologous temperatures above $0.3T_m$. This thermally induced movement of vacancies at room temperature (RT) promotes mutual recombination of vacancies and interstitials, resulting in a lower density of point defect clusters, which are seeds for the damage microstructure.

In particular, 5*xxx* and 6*xxx* series Al alloys exhibit a good combination of mechanical, thermal, corrosion resistance, and irradiation swelling resistance properties in a research reactor environment, which make these alloys a suitable choice for in-core structures and reactor vessel components of research reactors. The reactor vessel of the high flux reactor (HFR) in Petten has been fabricated from the aluminum alloy ASTM B209 [1], specification Al 5154–O with a restriction on Mg content to a maximum of 3.5 wt.%.

The components of these reactors can experience a large amount of neutron fluences, up to several 10^{27} n/m^2, during their operational life. For the HFR hotspot,[a] a maximum thermal fluence of ~20×10^{26} n/m^2 is expected by the end of 2025.[b] Substantial damage to the material's microstructure and mechanical properties can occur at these high fluence conditions. To this end, a dedicated SURveillance Program (SURP) is executed to understand, predict, and measure the influence of neutron radiation damage on the mechanical properties of the vessel material. As a part of SURP, a literature survey on irradiated Al alloys that are relevant for HFR vessel material is conducted to obtain fundamental understanding on expected mechanical property changes in relation with microstructural damage mechanisms, which forms the goal of this work.

This article is organized as follows. First, a brief review of various irradiation-induced damage mechanisms in Al alloys is presented. Next, the tensile data collected from the literature is analyzed to understand the contributions of various irradiation-induced damage mechanisms to the changes in the mechanical properties of these materials up to high irradiation fluences. Finally, the fracture toughness data from HFR SURP is compared with that of the literature, and the underlying damage mechanisms influencing fracture toughness properties are discussed to explain the suitability of literature data for the prediction of HFR SURP data beyond the current surveillance data.

2. Literature on irradiation effects in Al alloys

A substantial amount of literature is published on the irradiation behavior of Al alloys [2–11]. The available dataset on 6*xxx* series alloys is considerably larger due to their widespread use in several research reactors and cold-neutron sources [2, 4–10]. On the other hand, only limited data were found on 5*xxx* series alloys [3, 9, 11, 12]. The published data from the SURP of the HFR vessel are also included in this review [13]. Although 5*xxx* and 6*xxx* series alloys are

[a] Hotspot is the location on vessel wall where highest neutron fluence is received.

[b] Assuming that the irradiation conditions at the HFR hotspot are kept unchanged as they are in 2015.

fundamentally different in their microstructure and properties in unirradiated condition, the data on irradiated 6*xxx* series Al alloys have great relevance to 5*xxx* series data, because 5*xxx* series alloys slowly transform into 6*xxx* series alloys in the course of neutron irradiation due to the transmutation-produced Si content [9]. Therefore, this study is focused on both the 5*xxx* and 6*xxx* series types of Al alloys. The emphasis is on understanding the influence of neutron irradiation on mechanical and microstructural properties up to very high fluence values and, in particular, the effect of transmutation-produced Si content on the mechanical properties.

To help the discussion on differences in irradiation damage mechanisms in different Al alloys, a brief review on the differences in chemical composition and microstructure of 5*xxx* versus 6*xxx* series Al alloys is presented here. The microstructure of 6*xxx* series alloys is carefully engineered by a suitable age-hardening treatment to form coherent precipitates (GP zones and β″) within the matrix to obtain the required mechanical properties [14]. On the other hand, the as-produced 5*xxx* series has no precipitates within the matrix. The Mg solute atoms present in the solid solution provide the required strength properties. The composition of Al alloys of interest for the current discussion is shown in **Table 1**.

Alloy	Al	Mg	Si	Cu	Cr	Fe	Mn	Ti	Zn	Ni
5154 (HFR vessel)	Balance	3.10–3.50	≤0.25	≤0.05	0.15–0.35	≤0.40	≤0.10	0.10–0.20	≤0.20	–
5052	Balance	2.20	≤0.10	–	0.20	0.18	–	–	–	≤0.30
6061	Balance	0.80–1.20	0.40–0.80	0.10–0.40	0.04–0.35	≤0.70	≤0.15	≤0.15	≤0.25	–

Table 1. Chemical composition of different as-produced Al alloys in wt.%.

3. Irradiation-induced damage mechanisms in Al alloys

The damage caused by neutron irradiation is the major degradation mechanism leading to irradiation hardening and embrittlement of Al alloys used in Materials Test Reactors (MTRs). Both thermal and fast neutrons cause damage in Al alloys. Displacement damage by fast neutrons and transmutation damage by both thermal and fast neutrons are the two major damage mechanisms in irradiated Al alloys [3, 9, 10]. The relative contribution of these different damage mechanisms and the resulting impact on the mechanical properties depend on the alloy composition, thermal-to-fast fluence ratio (TFR), irradiation temperature, and other irradiation conditions.

3.1. Displacement damage

As in other metals, displacement damage is initiated by the production of primary knock-on atoms (PKAs) through elastic collision of fast (high energy) neutrons with the Al matrix. The resulting PKAs trigger displacement cascades leading to the formation of lattice vacancies, self-interstitial atoms, and dislocation loops. With increasing irradiation dose, dislocation

loops grow and encounter the other loops or dislocation network. When the loops interact with each other, they coalesce and contribute to the increase in network dislocation density. Interaction between individual dislocations and loops also contribute to the network.

The irradiation-induced dislocation density determines the extent of irradiation hardening and embrittlement resulting from displacement damage. It is known from literature that the dislocation density in irradiated metals evolves toward a saturation value with increasing dose [15]. This occurs when the dislocation annihilation rate reaches the value of the production rate. The resulting contribution of displacement damage to irradiation hardening and embrittlement remains nearly constant above the irradiation dose levels at which dislocation density reaches a saturation value. From that point onward, transmutation-produced Si plays a dominant role in contributing to irradiation hardening of Al alloys as discussed further in the next section. A detailed discussion on the evolution of displacement damage in Al alloys can be found in Refs. [9, 15].

3.2. Transmutation damage

Transmutation damage in aluminum can be caused by both fast and thermal neutrons. Fast neutrons produce gaseous products like He and H through (n, α) and (n, p) transmutation reactions [9]. On the other hand, thermal neutrons cause transmutation of Al into Si through the following sequential reactions,

$$^{27}\mathrm{Al}(n,\gamma)^{28}\mathrm{Al},\ ^{28}\mathrm{Al} \rightarrow {}^{28}\mathrm{Si} + \beta, \tag{1}$$

leading to an increase in Si content with increasing thermal neutron fluence. In most metals, the gaseous transmutation products play a larger role in the development of radiation damage microstructure than nongaseous transmutants. However, Al alloys used in MTRs are different in this respect. Depending upon the thermalization of the neutron spectrum, the solid transmutation product Si can have a stronger effect on radiation damage structure than gaseous transmutation products, as discussed in more detail in the following subsections.

3.2.1. Gaseous transmutation damage

Gaseous transmutation products can have a substantial influence on the radiation damage structure by promoting cavity formation and swelling. Gaseous transmutation products favor cavity nucleation by bubble formation at locations such as grain boundaries and stable particle–matrix interfaces, which otherwise are not suitable for nucleation of pure vacancy clusters.

It should be noted that the resistance to cavity formation and swelling differ between different types of Al alloys even in the presence of similar amounts of gaseous transmutation products. Alloys that promote trapping and recombination of point defects reduce vacancy supersaturation and hence exhibit increased resistance to cavity formation and swelling [3]. For instance, 5052-O and 6061 alloys have an excellent resistance to cavity formation and swelling, when compared to pure Al and grade 1100 alloys. Literature reports [16] show that the incubation

http://dx.doi.org/10.5772/63294

dose for cavity formation of 5052-O alloys, ~ 5×10^{26} n/m^2, is about 1000 times that of pure Al. Such strong resistance to cavity formation is imparted to the solute Mg present in the solid solution, which can act as trapping and recombination sites for vacancies and interstitials to reduce vacancy supersaturation [3]. Once the Mg is drawn from solution to form Mg_2Si precipitates, the trapping and recombination sites are presumably shifted to these Mg_2Si precipitates, whose high spatial density might provide overlapping point-defect capture zones. High concentrations of precipitates are expected to contribute to reduced swelling by trapping gases, making these gases not available for cavity nucleation. Farrell et al. [9] reported that the radiation swelling in 5052-O is only about 1% at a fast fluence of ~18×10^{26} n/m^2. The corresponding thermal fluence value is 31×10^{26} n/m^2 with about 7% of transmutation-produced Si. Only sparsely distributed voids are found in 5052-O microstructure at these high fluence values [9]. The contribution of voids to the increase in strength and decrease in ductility of this alloy is found to be negligible at this small amount of swelling [3]. No swelling data was published for 5154-O alloy in these conditions. However, due to the similarity in microstructures of both 5052-O and 5154-O alloys and matching irradiation conditions, a comparable swelling behavior can be predicted in 5154-O alloy at HFR vessel hotspot. Using the swelling data of 5052-O from Farrell et al. [9], the estimated swelling in 5154-O alloy will be ~0.3% for the projected HFR hotspot fluence values by the end of 2025. From these arguments, it can be concluded that the creation of voids and bubbles in 5*xxx* series alloys is not a crucial degradation mechanism for the expected hotspot thermal fluence values of HFR vessel by the end of 2025.

3.2.2. Solid transmutation damage

Transmutation-produced Si by thermal neutrons causes substantial radiation damage in Al alloys. Kapusta et al. [11] confirmed that the Si-content is a major indicator for the neutron irradiation effects on the basis of postirradiation testing of Al alloys containing 2.12% Si from transmutation. A quick estimate of the production rate of transmutation-produced Si (~0.084 wt.%/year of 270 effective full power days at HFR hotspot) can be obtained by multiplying the thermal fluence with the standard thermal neutron absorption cross section for Al (=230 milli barn (mb)) [9]. The solubility of Si in the Al matrix below 373 K is negligible. Hence, the transmutation-produced Si will either precipitate in elemental form as in pure Al, grade 1100 and 6061 alloys or forms Mg_2Si precipitates as in 5*xxx* series alloys until all the Mg in solid solution is consumed.

The structure, size, and distribution of these precipitates (Si and Mg_2Si) in the microstructure will determine the resulting mechanical properties of irradiated alloys. For a given volume fraction of precipitates in the microstructure, finer precipitates result in higher strength, but lower ductility and fracture toughness properties. The structure of the Mg_2Si precipitates in 5052 alloy irradiated to 9.7×10^{26} n/m^2 thermal fluence is found to be similar to the thermally aged Mg_2Si precipitates in 6*xxx* alloys [3]. However, irradiation-assisted Mg_2Si precipitates in 5*xxx* alloys are observed to be fine compared to precipitates in thermally aged 6061 alloy [9], probably because irradiation-assisted precipitation occurs at temperatures much lower than the thermal aging temperature of 433 K, thereby favoring a large number of nucleation sites.

In case of control rod drive follower (CRDF) A-2 tubes of the High Flux Beam Reactor (HFBR) in Brookhaven National Laboratory, USA, produced from 6061-T6 alloy, irradiated at 338 K up to a very high thermal fluence of 42 × 10^{26} n/m^2, a high concentration of very fine (8 nm) amorphous Si-rich particles are observed in the microstructure in place of original Mg_2Si precipitates [5]. The corresponding fast fluence is 2 × 10^{26} n/m^2, which gives a high TFR of 21 compared to the HFR hotspot TFR value of maximum 1.4. The total measured Si at this fluence was found to be ~8 wt.%, including 0.6% of the initial Si content.

The location of this transmutation-produced Si precipitates in the microstructure will have substantial impact on the mechanical properties of the alloys. In 1100 and 6061 alloys, it was identified that the transmutation-produced Si will precipitate as elemental Si particles, which are uniformly distributed in the matrix and associated with voids [9]. Farrell et al. [17] reported a noncrystalline Si-coating inside the voids of 1100-O Al alloy at a high thermal fluence (E < 0.025 eV) of ~2.3 × 10^{27} n/m^2. The 6061 alloy irradiated to ~10^{27} n/m^2 at ~328 K has shown a decoration of original Mg_2Si precipitates with transmutation-produced Si in addition to the association of Si particles with voids [9]. Precipitation of this Si along the grain boundary can lower the fracture toughness. For example, CRDF A-2 tubes of HFBR produced from 6061-T6 alloy have shown a drop in fracture toughness to ~8 (MPa)·m$^{1/2}$ from an unirradiated value of 21.75 (MPa)·m$^{1/2}$ after irradiation to a thermal neutron fluence of ~42 × 10^{26} n/m^2 at 338 K (see **Figure 4**). The microstructure of this alloy, with a very high transmutation-produced Si content of 8 wt.%, has shown large silicon flakes occupying less than one-fifth of the grain boundary area [5]. Similarly, heavy discontinuous precipitation at grain boundaries is observed in 5052 alloy irradiated up to a thermal fluence of ~31 × 10^{26} n/m^2 [3].

From the above discussion, it can be concluded that the transmutation-produced Si is the dominant irradiation damage mechanism in 5*xxx* and 6*xxx* series Al alloys irradiated at temperatures <373 K. Consequently, transmutation-produced Si is taken as the measure of the irradiation damage in HFR vessel wall. There are differences in how this transmutation-produced Si will influence the mechanical properties of 5*xxx* and 6*xxx* Al alloys, which will be discussed in the next section.

4. Discussion on irradiation-induced damage effects on mechanical properties of 5*xxx* and 6*xxx* series Al alloys

Although fracture toughness data on irradiated Al alloys is scarce, significant data on tensile properties is available in the literature. In this section, tensile data on irradiated Al alloys collected from literature is plotted as a function of thermal fluence to understand the changes in tensile properties with the evolution of irradiation-induced microstructural damage (or transmutation-produced Si content). Once this relation is established, then one can make a bridge to correlate these changes to corresponding changes in fracture toughness properties, where only limited data is published in the literature.

http://dx.doi.org/10.5772/63294

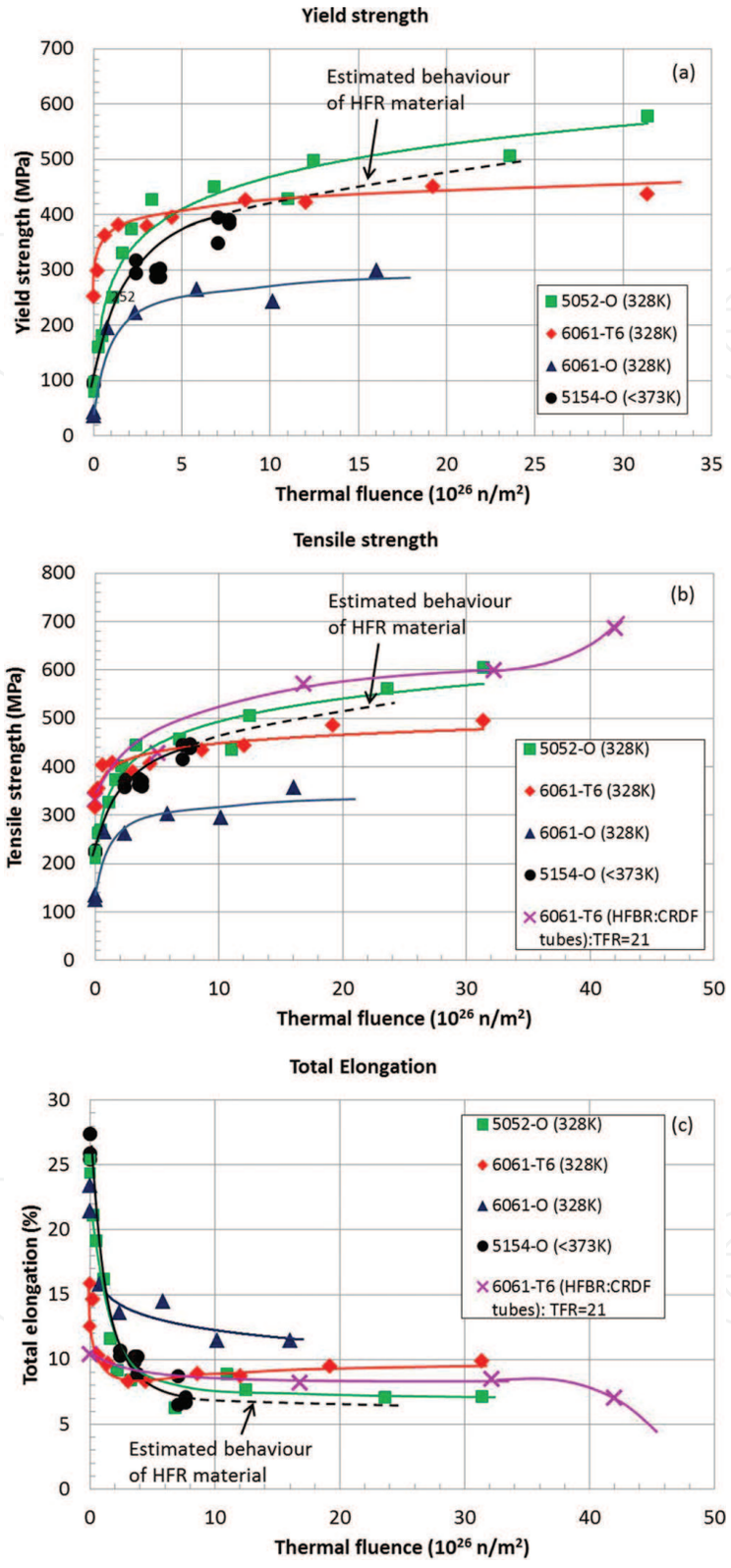

Figure 1. Literature tensile data of irradiated Al alloys in comparison with HFR SURP data. (a) Yield strength versus thermal fluence, (b) tensile strength versus thermal fluence and (c) total elongation versus thermal fluence.

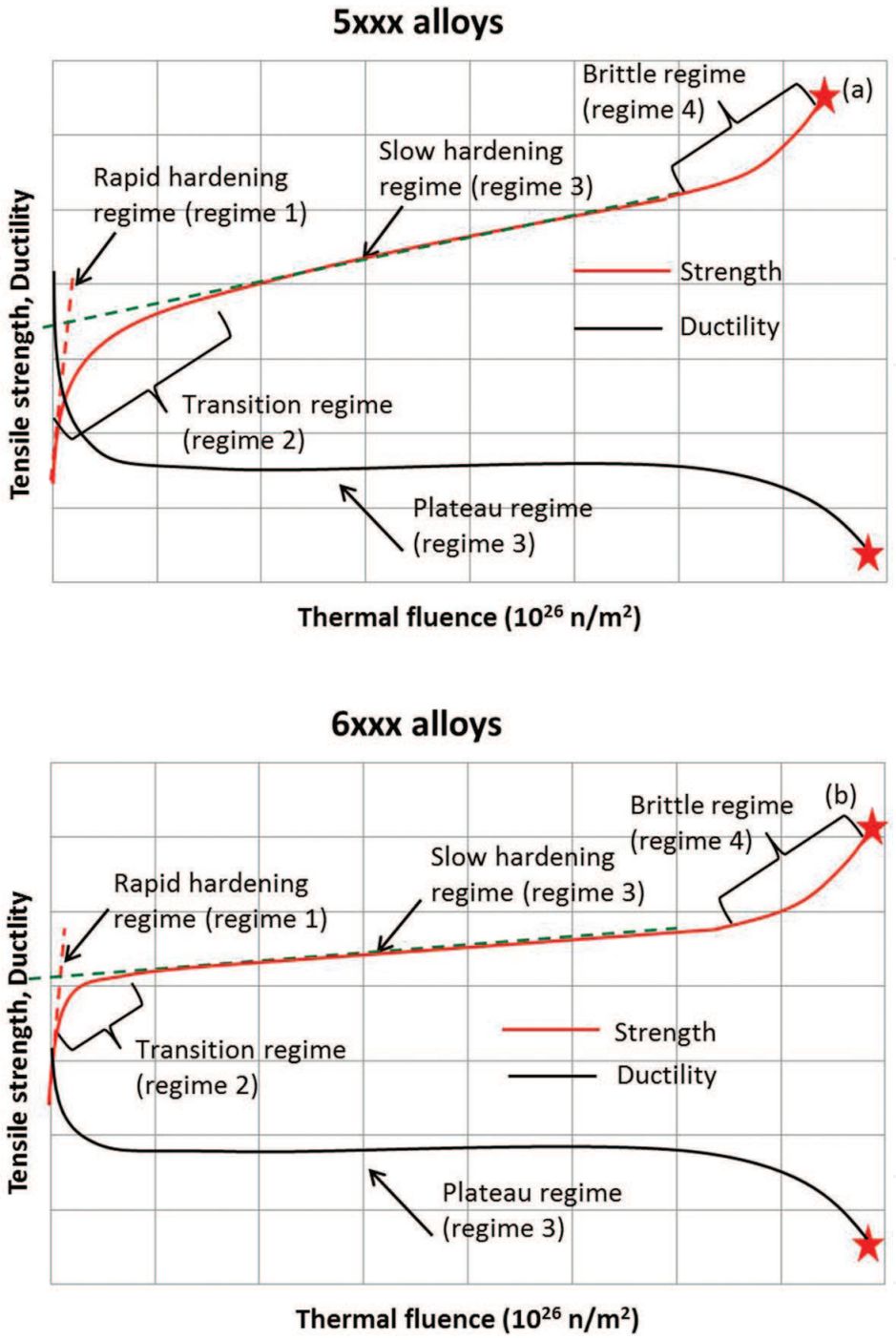

Figure 2. Schematic diagram showing various regimes in irradiation hardening behavior of (a) 5xxx and (b) 6xxx series Al alloys.

Farrell et al. [3] published data on tensile behavior of 5052-O aluminum alloy (Al–2.2% Mg) heavily irradiated in HFIR to fluences greater than 10^{27} n/m^2 in contact with cooling water at 328 K (see **Figure 1**). HFIR is predominantly a thermal reactor with a strong fast neutron component. The thermal neutron fluence ($E < 0.0025$ eV) of the samples ranged up to ~31 × 10^{26} n/m^2 to produce 7.15 wt.% Si. The fast neutron fluence ($E > 0.1$ MeV) is a factor of 1.7 (=TFR)

http://dx.doi.org/10.5772/63294

lower than the thermal fluence, and results in a damage value of 260 displacements per atom (dpa). Associated gas generation due to fast neutrons was estimated to be 8.5×10^{-5} atomic fraction He and 5×10^{-4} atomic fraction H. It is important to notice that this data is very relevant to the HFR SURP program because of the (i) similar chemical composition of 5052 and 5154 alloys, except that Mg in 5154-HFR alloy is 3.2% instead of 2.2% in 5052 and (ii) similar irradiation conditions, including temperature, TFR, and high fluence values. Farrell et al. [2] also published tensile data on heavily irradiated 6061-O and 6061-T6 alloys irradiated at 328 K up to ~31×10^{26} n/m^2 and tested at three different temperatures (323, 373 and 423 K). **Figure 1** shows only results at 323 K due to their relevance to HFR operating conditions. Additionally, tensile strength data from a 6061-T6 type alloy tested from CRDF A-2 tubes of HFBR, published by Weeks et al. [5] are also shown in **Figure 1**.

Comparison of yield and tensile strength properties of all these alloys including HFR-SURP tensile data, shown with added trend lines in **Figure 1 (a, b)**, reveals specific trends in irradiation hardening and embrittlement behavior. Each of these alloys showed a rapid hardening regime (and corresponding drop in ductility) at the beginning, followed by a transition regime toward a relatively slow hardening (and stable ductility) regime. A brittle regime is observed in some alloys at the end, as shown schematically in **Figure 2**. Depending on whether an alloy is of 5*xxx* or 6*xxx* series, a single or multiple irradiation damage mechanism can be active, determining the hardening rates in each of these regimes.

4.1. Tensile behavior of 6*xxx* series alloys

In case of 6*xxx* series Al alloys, rapid hardening observed at the onset of irradiation (regime 1), for example, curves of 6061-O and 6061-T6 alloys (**Figure 1 (a, b)**), can be attributed to irradiation-induced dislocation damage. It is known that the irradiation-induced dislocation density rapidly increases at the beginning and reaches a saturation value (see Section 3.1) at relatively low fluence values. For steels irradiated at 603 K (~$0.35T_m$), this saturation dislocation density is expected to reach around a fast fluence of ~2×10^{26} n/m^2 [15]. For Al alloys irradiated at temperatures about 323 K (~$0.35T_m$), it is expected that saturation is reached at lower fluences due to the low effective displacement energy of Al (~25 eV) compared to Fe (~40 eV) [9].

In the transition regime (regime 2), precipitation of transmutation-produced Si takes over as the major contributing mechanism, while the dislocation density reaches a saturation limit. It is known from literature that the transmutation Si in 6*xxx* alloys nucleate as amorphous Si particles in the matrix, associate with irradiation-induced voids, and decorate existing Mg_2Si precipitates (see Section 3.2). The contribution of this mechanism to irradiation hardening of 6*xxx* series alloys is low because deformation which occurs by the shearing of soft Si particles produces little strain hardening [18]. At the same time, the hardening contribution from an increase in size of existing Mg_2Si precipitates (due to Si decoration) is also low. This is because for a given particle density, the increase in precipitate size (r) and the decrease in planar spacing (λ) of the precipitates resulting from precipitate growth due to Si decoration have a minimal effect on strength based on the Orowan–Ashby equation [19] (Eq. (2)).

$$\Delta\sigma = \frac{0.13Gb}{\lambda}\ln\frac{r}{b} \tag{2}$$

Assuming a saturation density of ~ 6×10^{14} m^{-2} in Al alloys (same as in steel), a rough estimate of the total contribution of dislocation hardening can be made using the following equation [20]:

$$\Delta\sigma_{dis} = \sigma - \sigma_o = Gb\rho^{1/2}, \tag{3}$$

where σ is the strength of the material after introducing dislocation structure, σ_o is the intrinsic strength of the material with low dislocation density, G is shear modulus (=2.648×10^4 MPa), b is Burgers vector (0.286 nm) and ρ is dislocation density. The G and b values of pure Al taken from reference [21] are used here. Substituting $\rho = 6 \times 10^{14}$ m^{-2} into Eq. (3) gives $\Delta\sigma$ = ~186 MPa. The magnitude of hardening observed at the beginning of 6061-O and 6061-T6 alloys is in good agreement with this value. An estimation of the total irradiation hardening using the microstructure data (r = 4 nm, λ = 4 nm) of CRDF A-2 alloy at 42×10^{26} n/m^2 thermal fluence taken from [5] resulted in an estimated yield strength of 605 MPa, which is comparable to the available tensile data for this alloy.

A low hardening rate observed in regime 3 of these alloys can be solely attributed to the growth of existing precipitates. No further increase in the precipitate density occurs in this regime leading to a stable ductility. The final brittle regime (regime 4) with an increasing hardening rate and a decreasing ductility is observed only in 6061-T6 alloy (from CRD A-2 tubes of HFBR) at very high fluences. Although this alloy is the same as 6061-T6 alloy and irradiated at similar temperatures, a difference in behavior is observed due to irradiation at very high TFR, as explained in Section 4.4.

4.2. Tensile behavior of 5*xxx* series alloys

The differences in irradiation hardening trends in all four regimes of 5*xxx* and 6*xxx* series alloys are depicted schematically in **Figure 2**. Both 5052-O and 5154-O alloys show similar irradiation hardening and embrittlement behavior (**Figure 1**) due to similar alloy microstructure and irradiation conditions. The unirradiated strength values of 5052-O and 5154-O alloys are lower, and ductility is higher than 6061-T6 alloy (**Figure 1**) due to the absence of Mg_2Si precipitates before irradiation. In the rapid hardening regime, the magnitude of irradiation hardening and embrittlement in 5*xxx* series alloys is observed to be much higher than 6*xxx* series, because both dislocation hardening (due to displacement damage) and precipitation hardening (due to the formation of Mg_2Si precipitates from transmutation Si) occur simultaneously in 5*xxx* alloys (see Section 3.1).

The contribution of both mechanisms continues in the transition regime until dislocation damage reaches a saturation value (at <2×10^{26} n/m^2 of fast fluence or <4×10^{26} n/m^2 of ther-

mal fluence). Simultaneously, a saturation in the density of precipitates is expected to occur in this regime, leading to the formation of no new Mg_2Si precipitates.

With further irradiation, the hardening continues with a decreasing rate as Mg_2Si precipitates continue to grow until all the Mg is pulled out from the Al solid solution in the final slow hardening regime. Based on the stoichiometric analysis, production of 0.58 wt.% transmutation Si will consume 1% Mg in the alloy. That means all the Mg in 5154-0 alloy is consumed at ~1.85% transmutation Si (~8.66×10^{26} n/m^2 of thermal fluence) and in 5052-O alloy at ~1.27% transmutation Si (~5.95×10^{26} n/m^2 of thermal fluence).

With continued irradiation, the newly formed transmutation-produced Si either decorates existing precipitates (like in 6*xxx* series) or associates with voids, which are expected to form only at very high fast fluences in 5*xxx* alloys as explained in Section 3.2. The higher hardening rate observed in regime 3 of 5*xxx* alloys can be attributed to the higher density and volume fraction of Mg_2Si precipitates than that observed in 6*xxx* series alloys. A stable ductility is observed in this stage similar to 6*xxx* series alloys due to no further increase in precipitation density. In fact, a small decrease in particle density may occur in this regime due to particle coalescence during their growth. The opposite effects of a small decrease in particle density and a slow hardening due to precipitate growth on ductility could be compensating each other, leading to a plateau in the ductility behavior in regime 3. No brittle regime is observed in the available data of 5*xxx* alloys until a thermal fluence of 31×10^{26} n/m^2.

Similar to 6*xxx* alloys, a rough estimation of the total irradiation hardening contribution is performed for 5052-O and 5154-O alloys using Eq. (2) for the dislocation-hardening contribution and Eq. (3) for contribution from precipitation hardening. An average precipitate size of 10 nm and linear planar spacing between precipitates of 10 nm is used from the microstructure data presented in [3] on 5052-O alloy irradiated to a thermal fluence of 31×10^{26} n/m^2. This resulted in a total yield strength of 547 MPa (including unirradiated yield strength value of 85 MPa) for 5052-O, matching very well with the data presented in **Figure 1 (a)**. Similar analysis for 5154-O at a thermal fluence of 9.81×10^{26} n/m^2, with an average precipitate size of 8 nm and linear planar spacing between precipitates of 20 nm (obtained from **Figure 5**) [13] resulted in a total yield strength of 410 MPa, again matching with the trends seen in **Figure 1 (a)**.

4.3. Fracture toughness behavior of 5*xxx* and 6*xxx* series alloys

In this section, first the fracture toughness data from HFR SURP is plotted against the available literature data on highly irradiated Al alloys. The evolution of fracture toughness behavior of 5*xxx* and 6*xxx* alloys during neutron irradiation is discussed, and a connection is established between tensile and fracture toughness behavior in various regimes observed in the previous section.

4.3.1. Literature fracture toughness data of 5xxx series Al alloys

No additional data on fracture toughness properties of 5*xxx* Al alloys was found in the literature except the data from 5154-O alloy from HFR SURP [13]. The fracture toughness properties of the HFR surveillance specimens are periodically measured to assess and predict the hotspot behavior of HFR vessel in comparison with the vessel's fracture toughness design limit of 6 (MPa)·$m^{1/2}$ [22]. Fracture toughness properties of surveillance specimens from the current HFR vessel tested until 2010 are plotted as a function of thermal neutron fluence in **Figure 3 (a)**. The thermal neutron fluence is taken as an indicator for the measure of irradiation damage in HFR vessel material, because thermal neutrons are the major cause of damage by producing Si through transmutation, as explained in the previous sections. **Figure 3 (b)** shows the relation between the thermal fluence and transmutation Si in fracture toughness specimens tested in SURP.

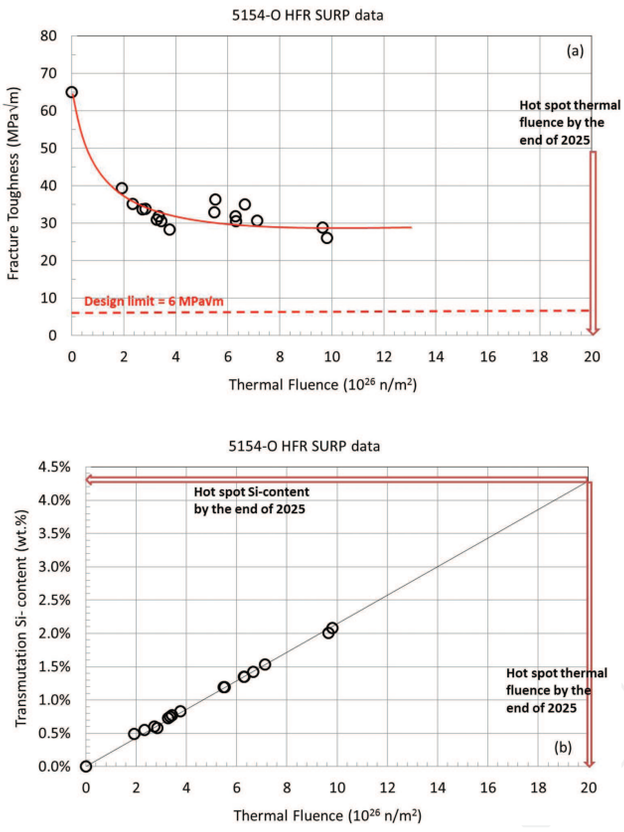

Figure 3. (a) HFR SURP fracture toughness data as a function of thermal neutron fluence. (b) Transmutation Si values as a function of neutron thermal fluence of fracture toughness samples tested in HFR SURP program. Note that the projected hotspot thermal fluence and Si content are based on the assumption that the irradiation conditions at the HFR hotspot are kept unchanged as they are in 2015.

4.3.2. Literature fracture toughness data of 6xxx series Al alloys in comparison with HFR SURP data

Only limited data was published on fracture toughness properties of irradiated Al alloys [5, 8, 10]. The most relevant data for the HFR (irradiation temperatures < 373 K) is plotted in

http://dx.doi.org/10.5772/63294

Figure 4 in comparison with HFR SURP data. Data from 6061-T6 alloy irradiated at < 373 K in the High Flux Isotope Reactor (HFIR) in Oak Ridge National Laboratory, USA matches quite well with the HFR SURP data. As it can be seen from **Figure 4**, there is one high fluence data point published by Weeks et al. [5] beyond the current surveillance data of the HFR vessel. This data is from the CRDF A-2 tubes of the HFBR in Brookhaven National Laboratory, USA, produced from 6061-T6 alloy, irradiated at 338 K up to a thermal fluence of 42 × 10^{26} n/m^2. The corresponding fast fluence of this data point is 2 × 10^{26} n/m^2, which gives a high TFR of 21, compared to the HFR hotspot TFR value of maximum 1.4. The total measured Si at this fluence was found to be ~8 wt.%, including 0.6% of initial Si content. The reported thermal fluence and Si content of this data point are approximately two times the estimated thermal fluence (~20 × 10^{26} n/m^2) and Si (~4.3 %) content of the HFR hotspot by the end of 2025. Note that this data is from the same material and at the same irradiation conditions for which the tensile data at very high thermal fluences (~42 × 10^{26} n/m^2) is also available (see **Figure 1**).

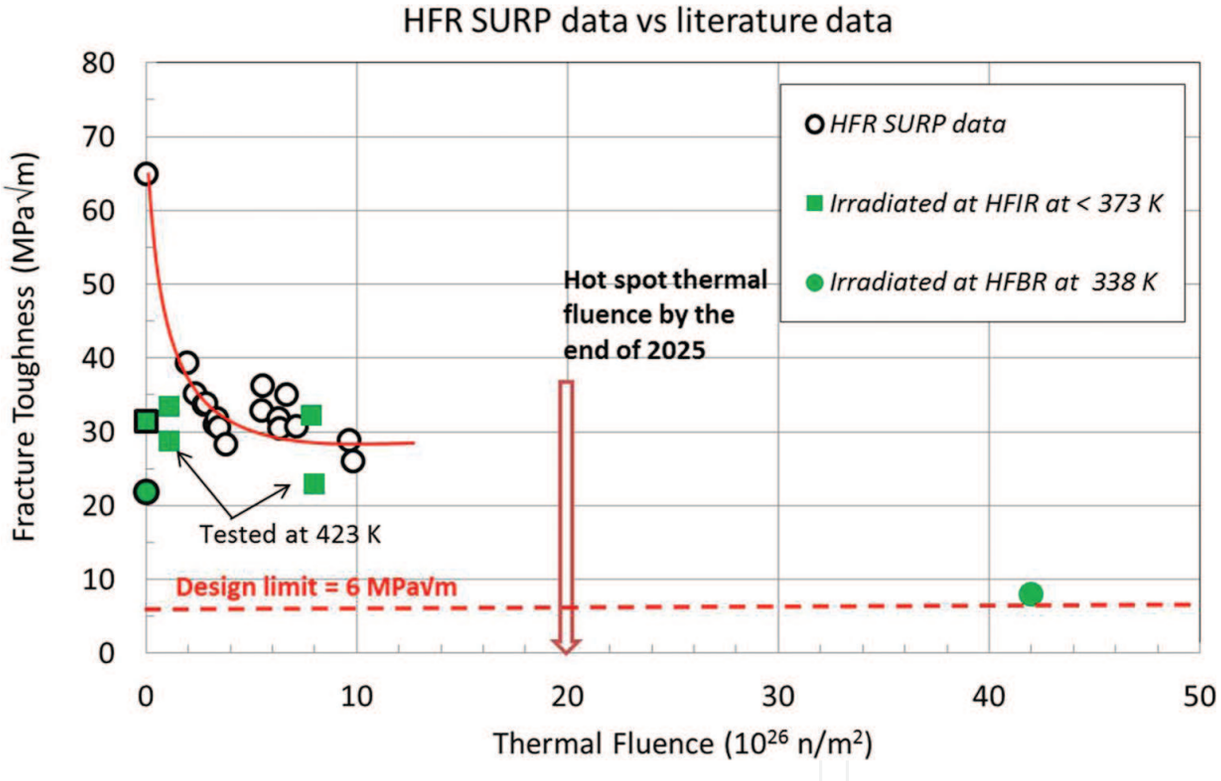

Figure 4. HFR SURP fracture toughness data in comparison with literature data [5,10].

4.3.3. Fracture toughness behavior of 5xxx and 6xxx series alloys

In the rapid hardening regime (regime 1), the fracture toughness value drops rapidly in line with the observed hardening and ductility behavior of 5*xxx* alloys (**Figure 3** vs. **Figure 1 (c)**).

This is because the hardening-induced embrittlement causes the decrease in both ductility and fracture toughness properties. In this regime, the magnitude of the drop in 5*xxx* alloys is high compared to 6*xxx* alloys, because both dislocation damage and precipitation damage mechanisms are active in 5*xxx* alloys, whereas only dislocation damage dominates in 6*xxx* alloys. This explains the sharp drop observed in fracture toughness of 5154-O alloy at the onset of irradiation compared to a shallow decrease in fracture toughness properties of 6061-T6 alloy in this regime (see **Figure 4**).

As the irradiation continues, both the dislocation density and the Mg_2Si precipitate density evolve toward a saturation limit describing the slow decrease of fracture toughness toward a plateau in the transition regime. Transmission electron microscopy results of precipitate microstructure reported in [13] are shown in **Figures 5** and **6**. From these results it can be seen that the saturation density is achieved at ~3 × 10^{26} n/m^2 of thermal fluence for 5154-O alloy of HFR vessel. Note that these pictures were taken using a "JEOL JEM-1200ex STEM/TEM" machine operating at 120 keV, located in JGL laboratory at NRG.

After that, the fracture toughness of 5154-O reaches a plateau at a thermal fluence of ~ 4 × 10^{26} n/m^2 after which no further increase in dislocation and precipitate density is expected (**Figure 3**). In fact, a small decrease in particle density may occur later in this regime due to particle coalescence during their growth. The opposite effects of a small decrease in particle density and a slow hardening due to precipitate growth on embrittlement could be compensating each other leading to a plateau in the fracture toughness behavior (similar to ductility) in regime 3. The behavior of 5154-O alloy is expected to be similar to 6*xxx* series alloys in this regime at similar irradiation conditions. This is because within this regime the irradiation hardening in both alloy types occurs primarily due to the growth of existing precipitates by newly produced transmutation Si. A close agreement between the fracture toughness data of 6061-T6 alloy irradiated in HFIR at <373K and HFR SURP data in the plateau regime (see **Figure 4**) confirms this theory.

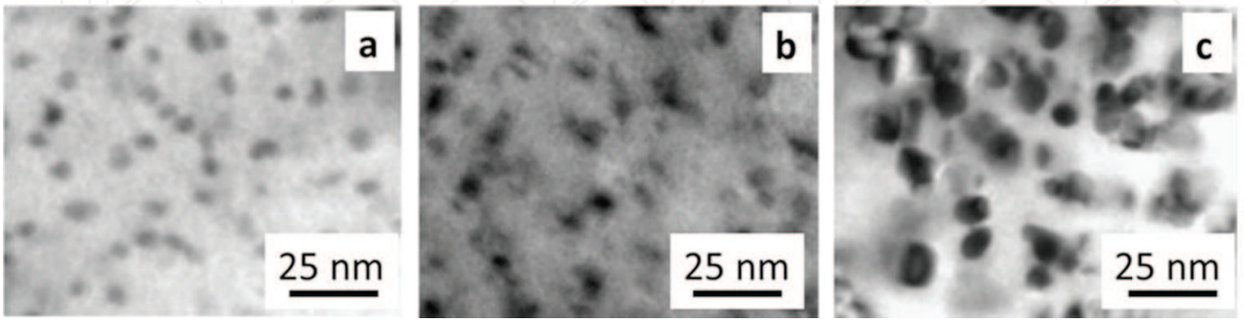

Figure 5. TEM images showing the evolution of precipitate size with thermal fluence in 5154-O Al alloy (HFR SURP specimens). (a) 2.73x1026 n/m2, 0.68 wt.% Si, (b) 3.76x1026 n/m2, 0.88 wt.% Si and (c) 9.81x1026 n/m2, 2.21 wt.% Si. (Photograph courtesy N.V. Luzginova et. al. [13])

http://dx.doi.org/10.5772/63294

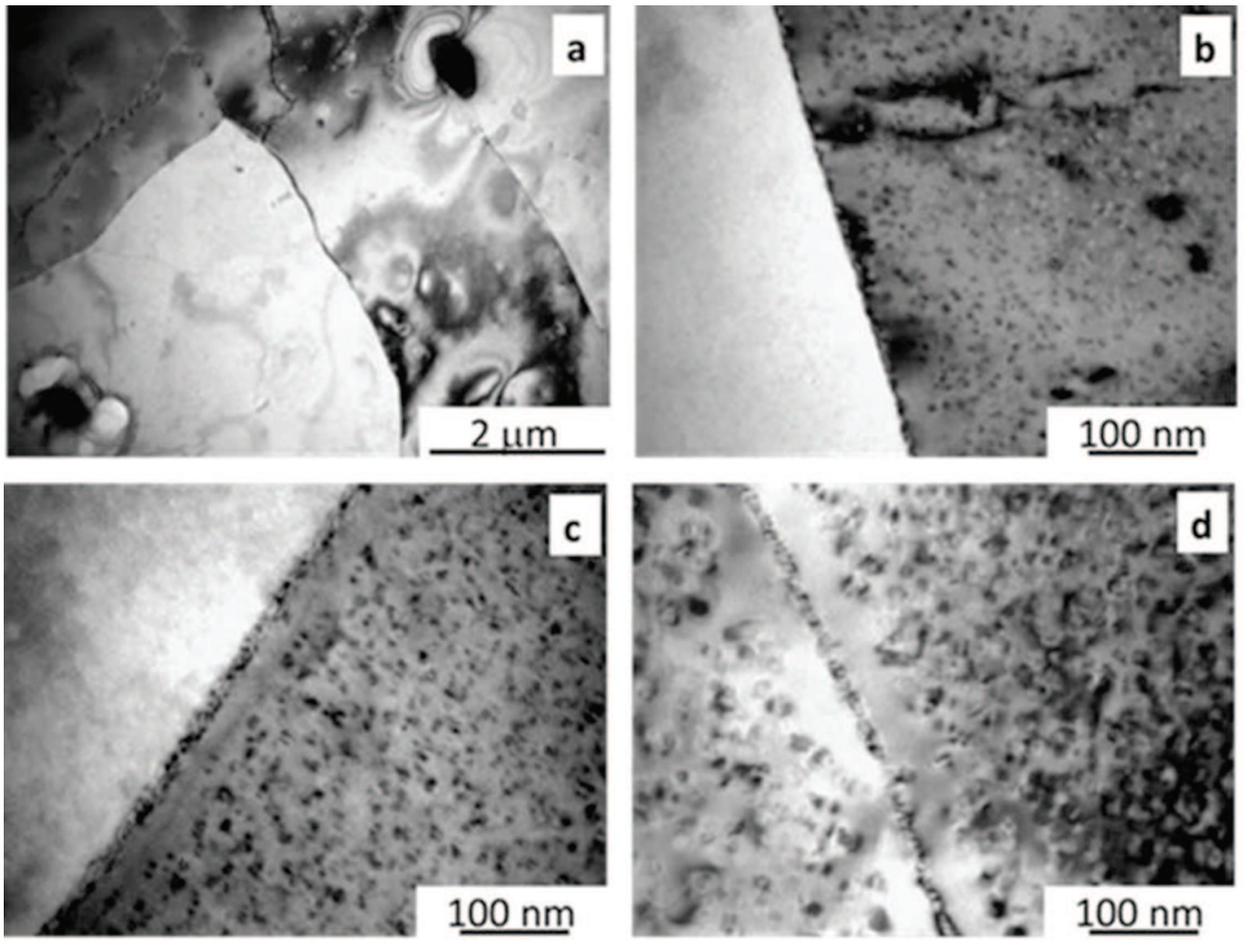

Figure 6. TEM images showing the evolution of precipitate microstructure with thermal fluence in 5154-O Al alloy (HFR SURP specimens). (a) Unirradiated, 0.04 wt.% Si, (b) 2.73×10^{26} n/m^2, 0.68 wt.% Si, (c) 3.76×10^{26} n/m^2, 0.88 wt.% Si, and (d) 9.81×10^{26} n/m^2, 2.21 wt.% Si. (Photograph courtesy N.V. Luzginova et al. [13].)

It is important to understand how long the plateau in the fracture toughness (or regime 3) will continue. This depends on the location of the precipitation of the transmutation Si. As already mentioned in Section 3.2.2, further increase in Si production to high values can lead to Si precipitation at grain boundaries. Fracture toughness value drops when the precipitation of Si at the grain boundaries cumulates to an extent that the dominant deformation and fracture mechanisms shift from the bulk microstructure to the grain boundaries. A heavy discontinuous precipitation observed at the grain boundary in 5052-O alloy at a thermal fluence of 31×10^{26} n/m^2 [3] has resulted in no substantial effects on ductility of this alloy. This suggests that the nature of fracture at these high fluence is still controlled by bulk deformation mechanisms (instead of mechanisms controlled by grain boundaries). Due to the similarity in 5154-O and 5052-O alloys (and irradiation conditions), the ductility and fracture toughness properties of the 5154-O alloy are also expected to show a plateau until such high fluences. Indeed, the observation of significant amount of micron-scale dimples on the fracture surface of 5154-O alloy irradiated to a thermal fluence of 9.81×10^{26} n/m^2 (**Figure 7**) proves that similar behavior can be expected from the 5154-O alloy [13].

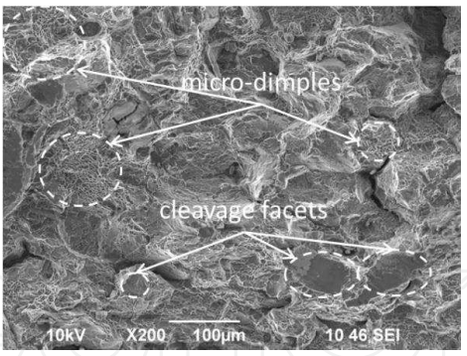

Figure 7. Fracture details of 5154-O alloy with a crack-tip thermal fluence of 9.81×10^{26} n/m^2. Figure shows fracture surface characterized by dominant microdimples and some cleavage facets [13].

CRDF A-2 tubes of HFBR produced from 6061-T6 alloy have shown a fracture toughness value of ~8 (MPa)·m$^{1/2}$ after irradiation to a much higher thermal neutron fluence of ~42×10^{26} n/m^2 at 338 K (see **Figure 4**). The decrease in fracture toughness from an unirradiated value of 21.75 (MPa)·m$^{1/2}$ for this alloy is primarily attributed to the following: (i) formation of very fine (~8 nm) Si-rich precipitates in the grains due to high TFR of 21 (as explained in Section 4.4) and (ii) large silicon flakes occupying about one-fifth of the grain boundary area at this high transmutation-produced Si content of 8 wt.% [5]. Fracture surface of this alloy revealed substantial intergranular separation with some residual ductility indicating that the contribution of grain boundary fracture mechanisms is increased at such high fluence values to enter into the brittle regime (regime 4).

From the above discussion, no differences in the evolution of irradiation damage at high fluences (in regime 3 and 4) are expected between 5*xxx* and 6*xxx* alloys due to differences in their initial chemical composition and microstructure. Moreover, the difference in the TFR of HFR SURP data and literature data is conservative as explained in the next section. This allows the use of published fracture toughness literature data of 6061-T6 Al alloys to predict the fracture toughness behavior of 5154-O Al alloy of HFR vessel at high fluences.

4.4. Effect of thermal-to-fast flux ratio (TFR)

It is known from the literature that a high difference in TFR can have substantial effect on irradiation hardening and embrittlement behavior of the same material [5]. It was highlighted in [3] that both the thermal and fast neutrons play independent and important roles leading to microstructural damage and corresponding property changes. A very high TFR, ranging from 80 to 500, could explain the observed craze-cracking in AG3-NET alloy (Al–3% Mg) beam tubes in the Reactor Haut Flux (RHF) at Grenoble [23]. Lijbrink et al. [12] pointed out that fast neutron flux reduces the effectiveness of the Si precipitation hardening process. A possible explanation for this behavior (as given in [5, 12]) is as follows. Fast flux has two opposite effects on precipitation:

i. The kinetic energy supplied by fast flux temporarily increases the solubility limit of Si in the matrix and opposes the condensation requirements for the precipitation.

http://dx.doi.org/10.5772/63294

ii. Local energy needed for jumping the nucleation barrier can be readily supplied by the fast flux.

However, the fast flux can be destructive when a freshly formed nucleus is hit by fast neutron collision. That means, at equal thermal fluence values, Si precipitation hardening is more effective at higher TFR. This leads to finer precipitate distribution, causing higher irradiation hardening, lower ductility, and eventually lower fracture toughness values at higher TFR. Indeed, the higher hardening rate observed in 6061-T6 alloy from CRDF A-2 tubes of HFBR irradiated at TFR of 21 compared to the similar 6061-T6 alloy irradiated in HFIR at TFR of 1.7 explains this behavior (**Figure 1 (b)**). Consequently, the high fluence data point from CRDF A-2 of HFBR at TFR = 21 (>>0.8–1.4 for HFR hotspot), shown in **Figure 4**, is likely to give a conservative estimation of the fracture toughness value under HFR conditions.

5. Summary and conclusions

A literature review on highly irradiated 5*xxx* and 6*xxx* series Al alloys is conducted to understand the expected changes in mechanical properties of HFR vessel material in relation with microstructural aspects beyond the current surveillance data to support the HFR SURP program. It was found that the irradiation swelling in 5*xxx* series alloys is not a crucial degradation mechanism for the expected hotspot fluence values of HFR vessel by the end of 2025. Dislocation damage is expected to reach a saturation limit at relatively low fast-fluence values. The damage caused by precipitation of transmutation Si is found to be the dominant mechanism affecting the fracture toughness properties of irradiated 5*xxx* and 6*xxx* series Al alloys at high thermal fluence values. Tensile and fracture toughness data collected from the literature up to very high thermal fluences is analyzed in comparison with the available HFR surveillance data. The observed changes in mechanical properties are classified into four different regimes.

The contribution of various irradiation damage mechanisms to the evolution of microstructure and mechanical properties is discussed in all four regimes for 5*xxx* and 6*xxx* series alloys. A rapid hardening regime characterized by a sharp drop in ductility and fracture toughness is observed at the onset of irradiation. In this regime, a higher degree of embrittlement is observed in 5*xxx* series due to the formation of Mg_2Si precipitates in addition to the contribution from dislocation damage. On the other hand, the hardening and embrittlement observed in regime 1 of 6*xxx* series alloys is primarily due to dislocation damage. The contribution from the precipitation of transmutation Si is estimated to be minor for 6*xxx* alloys in this regime. The contribution of both mechanisms continues in the transition regime (regime 2) for both alloy types, until both dislocation damage and precipitate density evolve toward a saturation value. Due to this, a lowering in irradiation hardening rate and correspondingly a slow decrease in ductility and fracture toughness toward a stable value are observed in this regime. Regime 3 is characterized by a plateau in ductility and fracture toughness values, due to no further increase in dislocation and precipitate density. A slow hardening observed in this regime is primarily due to the growth of existing precipitates. The behavior of 5*xxx* alloys is found to be

similar to 6*xxx* series alloys when irradiated under similar conditions in this regime. A final regime (regime 4) with an increasing hardening rate and a decreasing ductility indicates that the contribution of grain boundary fracture mechanisms increases at such high fluence values to enter into the brittle regime (regime 4).

For the 5154-O alloy at the hotspot irradiation conditions, regime 1 ends at ~2 × 10^{26} n/m^2. Regime 2 is observed between ~2 × 10^{26} and ~4 × 10^{26} n/m^2. Finally, the plateau in regime 3 starts at ~4 × 10^{26} n/m^2 and is expected to continue up to very high thermal fluences, that is, greater than the estimated hotspot thermal fluence by the end of 2025 (~20 × 10^{26} n/m^2). This is because for a 5052-O alloy, which was irradiated at similar conditions as HFR hotspot and resembles the alloy microstructure and composition of 5154-O, a plateau in ductility was observed from a thermal fluence of ~4 × 10^{26} n/m^2 until ~31 × 10^{26} n/m^2. It should be noted that the estimated HFR hotspot thermal fluence by the end of 2025 (~20 × 10^{26} n/m^2) is only two-thirds of the studied 5052-O alloy.

Additionally, high fluence fracture toughness data is found from the CRDF A-2 tubes of the HFBR in Brookhaven National Laboratory, USA, produced from 6061-T6 alloy, irradiated at 338 K, up to 42 × 10^{26} n/m^2. The corresponding fast fluence of this data point is 2 × 10^{26} n/m^2, which gives a high TFR of 21 compared to the HFR hotspot TFR value of maximum 1.4. The reported thermal fluence and Si content of this data point are approximately two times the estimated thermal fluence (~20 × 10^{26} n/m^2) and Si (~4.3%) content of the HFR hotspot by the end of 2025. Knowing that the transmutation-produced Si induces major damage to the microstructure of irradiated Al alloys, this high fluence data point from CRDF A-2 of HFBR is likely to give a conservative estimation of the fracture toughness value under HFR conditions due to irradiation of this alloy at much higher TFR (leading to high embrittlement) and negligible differences in the embrittlement behavior of 5*xxx* and 6*xxx* series alloys in the plateau regime.

From the above observations of literature tensile and fracture toughness data on irradiated Al alloys, one can conclude that the probability of the fracture toughness of HFR hotspot to fall below the design limit is negligible up until the currently estimated hotspot thermal fluence at the end of 2025.[c]

Acknowledgements

The work presented in this article is performed as a part of SURveillance Program (SURP) of HFR vessel with the financial support of NRG. The author thanks Dr. O. Wouters and Ir. T.O. van Staveren for useful discussion and critical review of this work. The author also acknowledges Dr. C. Li for helping in the extraction of data from the literature.

Export control note

[c] Assuming that the irradiation conditions at the HFR hotspot are kept unchanged as they are in 2015.

The content within this chapter is classified with the code EU DuC = N. EU DuC means European dual use code.

Author details

Murthy Kolluri

Address all correspondence to: kolluri@nrg.eu

Nuclear Research and Consultancy Group (NRG), The Netherlands

References

[1] ASTM-B209. Standard Specification for Aluminum and Aluminum-Alloy Sheet and Plate: ASTM International; West Conshohocken, PA, USA. 2007.

[2] Farrell K, King RT. Tensile Properties of Neutron-Irradiated 6061 Aluminum Alloy in Annealed and Precipitation-Hardened Conditions. ASTM STP 683; West Conshohocken, PA, USA. 1979. pp. 440–449.

[3] Farrell K. Microstructure and tensile properties of heavily irradiated 5052–0 aluminum alloy. J. Nucl. Mater. 1981; 97(1–2): 33–43.

[4] Weeks JR, Czajkowski CJ, Tichler, PR. Effects of High Thermal and High Fast Fluences on the Mechanical Properties of Type 6061 Aluminum in the HFBR. ASTM STP 1046; West Conshohocken, PA, USA. 1990. pp. 441–452.

[5] Weeks JR, Czajkowski CJ, Farrell K. Effects of High Thermal Neutron Fluences on the 6061 Aluminum. ASTM STP 1175; West Conshohocken, PA, USA. 1993.

[6] Munitz A. Mechanical Properties and Microstructure of Neutron Irradiated Cold-Worked Al-1050 and Al-6063 Alloys. Annual Report. IAEC; 1998. Online: http://www.iaea.org/inis/collection/NCLCollectionStore/_Public/31/027/31027808.pdf

[7] Munitz A, Shtechman A, Cotler C, Talianker M, Dahan S. Mechanical properties and microstructure of neutron irradiated cold worked A1-6063 alloy. J. Nucl. Mater. 1998; 252: 79–88.

[8] Yahr GT. Prevention of nonductile fracture in 6061-T6 aluminum nuclear pressure vessel. J. Press. Vessel Technol. 1997; 119(2): 150–156.

[9] Farrell K. Performance of aluminum in research reactors. In: Comprehensive Nuclear Materials. Editor: Konings RJM, Elsevier; Oxford. 2012. pp. 143–157.

[10] Farrell K. Assessment of Aluminum Structural Materials for Service within the ANS Reflector Vessel. ORNL Report. Report No. ORNL/TM-13049; DOE TN (United States) 1995.

[11] Kapusta B, Sainte-Catherine C, Averty X, Campioni G, Ballagny A. Mechanical characteristics pf 5754-NET-O aluminum alloy irradiated up to high fluences: Neutron spectrum and temperature effects. In: Joint Meeting of the National Organization of Test, Research, and Training Reactors and the International Group on Research Reactors. September 12–16, 2005; Gaitherburg.

[12] Lijbrink B, Grol HJV, Dekker F, Witzenburg WV. Effects of neutron irradiation on the mechanical properties of A 5154-O type aluminum alloy. ASTM STP 782; West Conshohocken, PA, USA. 1982. pp. 765–778.

[13] Luzginova NV, Nolles H, van den Berg F, van den Idsert P, van der Schaaf B. Surveillance program results for the high flux reactor vessel material. Effects Rad. Nucl. Mater. 2014; 26: 30–41.

[14] Murayama M, Hono K. Pre-precipitate clusters and precipitation processes in Al-Mg-Si alloys. Acta Mater. 1999; 47(5): 1537–1548.

[15] Was GS. Fundamentals of Radiation Materials Science. Berlin, Heidelberg, New York: Springer; 2007.

[16] Packan NH. Fluence and flux dependence of void formation in pure aluminum. J. Nucl. Mater. 1971; 40(1): 1–16.

[17] Farrell K, Bentley J, Braski DN. Direct observation of radiation-induced coated cavities. Scripta Metal. 1977; 11(3): 243–248.

[18] Dieter GE. Mechanical Metallurgy. In: Bacon D, editor. McGraw-Hill; 1988. Mechanical Metallurgy, McGraw-Hill, Cornell University, USA.

[19] Hart EW. Theory of dispersion hardening in metals. Acta Metal. 1972; 20(2). pp 275–289

[20] Reed-Hill R. Physical Metallurgy Principles. Van Nostrand; the University of Michigan, USA 1973.

[21] Farrell K, Richt AE. Microstructure and tensile properties of heavily irradiated 1100-O aluminum. In: Symposium on Effects of Radiation Structural Materials. STP 683; 1979. pp. 427–439.

[22] Ketema DJ, van der Schaaf B. Principles of HFR Vessel Surveillance Program—revE. Report No. NRG-25146/10,103852; Petten, The Netherlands, Publisher: NRG (internal report) 2011.

[23] Farrell K. Materials Selection for the HFIR Cold Neutron Sources. Report No. ORNL/TM-99-208; TN (United States), DOE 2001.